International Journal of GEOMATE, Sept., 2020, Vol.19, Issue 73, pp. 82– 90
ISSN: 2186-2982 (P), 2186-2990 (O), Japan, DOI: https://doi.org/10.21660/2020.73.25272
Geotechnique, Construction Materials and Environment

DEGRADATION OF MILD STEEL IN ETHANOL BURNING ENVIRONMENT: OXIDATION KINETICS AND MICROSTRUCTURAL ASPECT

* Sugiyanto[1], Mohammad Badaruddin[2]

[1,2]Department of Mechanical Engineering, Faculty of Engineering, Universitas Lampung, Indonesia

*Corresponding Author, Received: 08 March 2020, Revised: 29 March 2020, Accepted: 06 April 2020

ABSTRACT: The isothermal oxidation of an AISI 1005 steel (mild steel) in water vapour and CO_2 mixtures containing environments resulted from ethanol combustion had been investigated for exposure times ranging from 1 hour to 49 hours at elevated temperatures (700 °C, 750 °C and 800 °C). The steel was also oxidized in dry air for comparison. In water vapour and CO_2 environments, mild steel underwent a significant degradation in term of the oxidation kinetics compared with those of steel oxidized in dry air environment. This finding is supported by a lower activation energy for steel oxidized in ethanol combustion products (199 kJ/mol) than that of for steel oxidized in dry air (224 kJ/mol). In addition, the breakaway oxidation was found for the steel subjected to ethanol combustion products at 800 °C. The carbon deposited in the magnetite layer was believed to lead the breakaway oxidation after an exposure time for 4 hours. A typical iron oxide growing on steel oxidized in ethanol combustion product is a pyramidal grain structures with compact scale but in dry air environment the iron rich oxide growing on the steel surface is a wrinkle characteristic displaying hollow structures at 700 °C and rough-grained oxide structures at 750–800 °C.

Keywords: Low carbon steel, Ethanol combustion, Pyramidal grain, Carbon deposition

1. INTRODUCTION

The energy demand from fossil fuels has recently increased in the transportation sectors which lead to alternatively use the fuel by blending ethanol with fossil fuel in Worldwide. In addition, an additional ethanol into fossil fuel i.e. gasoline was intentional to reduce greenhouse gas emissions and consumption of fossil fuel [1]. As reported by Ashraf that ethanol-methanol and gasoline hybrids for vehicle can increase an engine performance and decrease an emission gasses containing of CO and NOx [2]. In addition, ethanol added to fossil fuels gives beneficial effect without resulting of knocking phenomenon in an engine [3]. Generally, ethanol as a replacement for methyl tertiary butyl ether (MTBE) is added into a gasoline as additive fuel at approximately 11–14% to enhance the octane number and reduce concentration of harmful substances in exhaust system [4–6]. However, ethanol-gasoline blending used for vehicle fuel produced amount of water vapour and CO_2 gasses.

Low carbon steel (mild steel) is suitably material for exhaust gas system in vehicle because its price is cheaper than stainless steel alloys [7]. However, the presence of water vapour and CO_2 mixtures in the exhaust components of vehicle have significant effects with respect to the oxidation resistance of exhaust materials [8–10]. Yuan et al. [11] confirmed that steel with 0.011 wt.% carbon content experienced severe oxidation attack in water vapour and oxygen environments, indicted by the linear oxidation kinetics behavior. Furthermore, Wang et al. [12] reported that there is a significant effect of CO_2 corrosion at a temperature up to 200 °C in pipe component manufactured from N86 and J55 steel grades. A few studies of high temperatures oxidation for mild steel in water vapour and CO_2 mixtures are available in literature. Therefore, it is important to verify the impact of ethanol combustion resulted water vapour and CO_2 gasses on the oxidation resistance of mild steel used as one of candidate material for exhaust components.

In the present work, we focused on an investigation of high-temperature oxidation of mild steel with grade AISI 1005. The performance of mild steel was carried out by exposing to ethanol combustion and to dry air at elevated temperatures (700 °C, 750 °C and 800 °C). Oxidation kinetics and the parabolic kinetics rate constant (k_p) were determined by weight gain changes and curve fitting method, respectively. Iron oxide scale morphologies, scale phases, fractural scale and an elemental compositions (at.%) in oxide scale were characterized by means of optical microscope (OM), X-ray diffraction (XRD) measurements, scanning electron microscopy (SEM) with energy dispersive spectroscopy (EDS). Quantitative and qualitative data obtained were used to elucidate an insight into mild steel oxidation mechanisms.

2. EXPERIMENTAL PROCEDURE

2.1. Material and Specimen Preparation

A low carbon steel, Grade AISI 1005 with the chemical composition of Fe-0.06C-0.35Mn-0.04P-0.05S (wt.%), was cut into coupons with dimensions of 20 mm × 10 mm × 2 mm to provide specimens according to ASTM standard G54 [13]. Total 90 pieces specimens were provided for oxidation tests in the present work. All specimen surfaces were mechanically ground with abrasive paper from 1000 to 2500-grits, and then cleaned used by ultrasonic cleaning in acetone.

2.2. Isothermal Oxidation Test

A respective three specimens were used for oxidation tests at each temperature and time oxidation given. A tube alumina chamber was used for conducting oxidation tests at elevated temperatures (700 °C, 750 °C, and 800 °C). Specimens were inserted and suspended in a crucible ceramic boat using a hook made of Grade 304 stainless steel wire and then placed in the hot zone. The specimen surface was perpendicular to the direction of air flow. Oxidation tests were conducted at elevated temperatures for exposure times ranging from 1 hour to 49 hours. Water vapour and CO_2 mixtures in a tube chamber were resulted from bioethanol burning products at elevated temperatures Air (as carrier gas) at a rate of 200 mL/min resulted by mini compressor was passed through a closed ethanol bath and then flown into the tube furnace. The temperature of ethanol in bath was maintained at 30 °C. The ethanol perfectly combusted in the tube chamber at elevated temperatures without resulting soot products. After a given isothermal oxidation time, specimens were taken out and cooled in room temperature. The analytical balances (PW 254 Adam series, UK) with a readability of 0.1 mg was used for weighing a specimen before and after oxidations tests. Each weight gain data for an oxidation kinetics was obtained from different specimens and an average value with respect to oxidation time at different temperatures were plotted in weight-gain (mg cm^{-2}) versus oxidation time, t (hour). In addition, plot of weight-gain data versus square root of oxidation time ($s^{1/2}$) was constructed for determining the parabolic kinetics constant, k_p (g^2 cm^{-4} s^{-1}) using a curve fitting method [7].

2.3. Sample Characterization

The specimens' structures of scale and phases formation were identified by X-ray diffractometer (RIGAKU RTD 300) using monochromatic Cu-Kα radiation operating at 40 kV and 100 mA. The X-ray diffraction (XRD) measurements were performed using a goniometer at scanning range of $20° \leq 2\theta \leq 80°$ using stepwise of 0.05°. The cross-sections and surface morphologies of the specimens were examined using optical Olympus microscope (OM) and JSM-6390 scanning electron microscopy (SEM) with backscattered electron image (BEI) and secondary electron image (SEI) signals operating at 20 kV, and energy dispersive spectroscopy (EDS) using spectrum range of 0–20 keV for a 50 s.

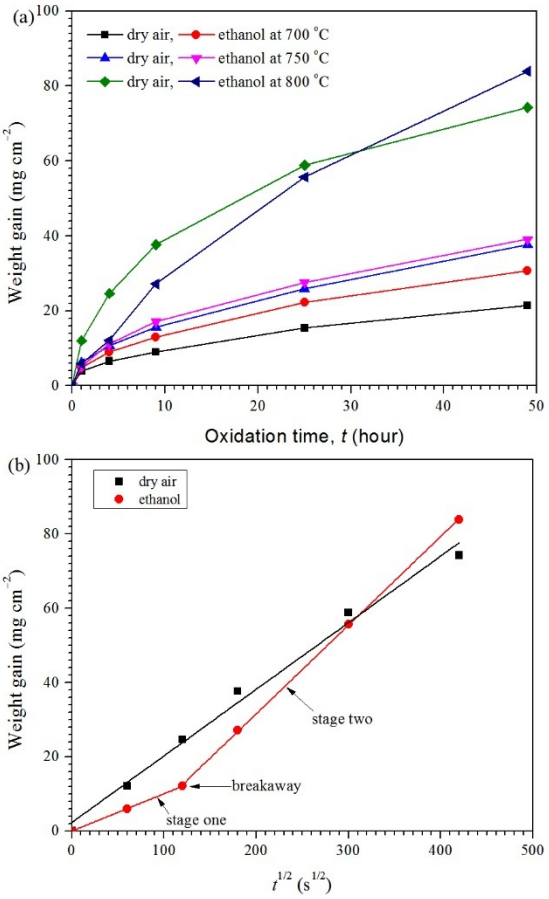

Fig. 1 (a) plot weight gain with oxidation time data series at elevated temperatures and (b) plot of weight gain with respect to square root of oxidation time ($t^{1/2}$) for AISI 1005 steel oxidized in dry air and ethanol at 800 °C for 49 hours

3. RESULTS AND DISCUSSION

3.1 Oxidation Kinetics

The presence of H_2O-CO_2 generated by ethanol combustion at 700–800 °C greatly affects the oxidation kinetics of the AISI 1005 steel, as shown in Fig. 1a. The weight gain of the specimen exposed to ethanol combustion is faster than all specimens exposed to dry air atmospheres at 700–800 °C for 49 hours. At 700 °C for 49 hours, the weight gain increased by a factor of 43.89% in ethanol combustion compared to the same steel oxidized in

dry air. For the steel oxidized in ethanol combustion, the trend curves of oxidation kinetics are similar to the steel oxidized in dry air at 700 and 750 °C. The ethanol combusted in the chamber possibly generated oxygen excess at these temperatures and thus the reaction of steel with O_2 and H_2O is similar to steel oxidized in O_2-H_2O-vapour gases mixtures [7–12].

As temperature was increased to 750 °C, the weight gain of specimen exposed to ethanol combustion showed an increase of 3.93% compared with the steel exposed to dry air (Fig. 1a). However, for 4 hours exposure, the increase of weight gain was slightly similar with specimens oxidized in dry air. The weight gain increases greatly for 9 hours at 800 °C. The weight gain of specimen exposed to ethanol combustion are much greater than those of dry air specimens by a factor of 11.76%.

The parabolic kinetics rate constant (k_p) are displayed in Table 1. The oxidation regimes for specimens oxidized in ethanol at 800 °C show differences in characteristic oxidation behaviors for short-term and long-term oxidation periods (Fig. 1b). The oxidation regimes were typically divided into two parts: (1) a first stage oxidation region (slow oxidation rate) and (2) a second oxidation regime (where the breakaway oxidation occurred). At 800 °C, the ethanol combustion product considerably produced H_2O and CO_2 gasses with low-pO_2, and therefore the presence of H_2O–CO_2 mixtures induced an acceleration of steel oxidation after a longer oxidation period. For oxidation kinetics law in stage one with a kinetics rate of 2.16 × 10^{-8} g^2 cm^{-4} s^{-1}, but an oxidation time of 4 hours, the kinetics rate increased by a factor of 2.43.

Table 1 The value of k_p (unit in g^2 cm^{-4} s^{-1}) for AISI 1005 steel

Environment	Temperature (°C)			Energy activation (kJ/mol)
	700	750	800	
Dry air	2.63×10^{-9}	7.83×10^{-9}	3.49×10^{-8}	224
Ethanol	5.23×10^{-9}	1.05×10^{-8}	5.24×10^{-8}	199

It had been reported previously that the kinetics constant of low carbon steel in an atmosphere containing a gas composition of 1%O_2–10%CO_2–3%H_2O–N_2 at 900 °C for 0.83 hours was found to be 5. 01 × 10^{-8} g^2 cm^{-4} s^{-1} [9], which is very similar to those values reported in this study for a similar low carbon steel exposed to ethanol at 800 °C for oxidation times 4–49 hours.

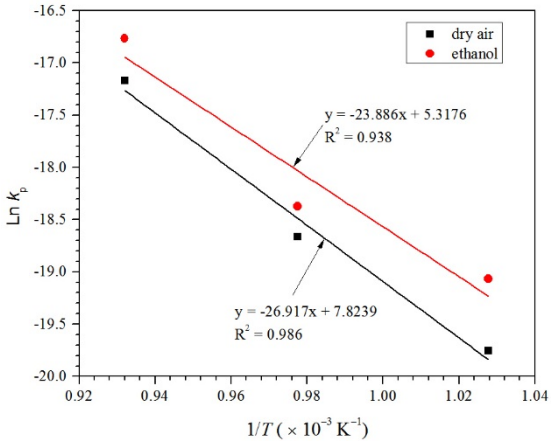

Fig. 2 Arrhenius plots of oxidation parabolic rates for AISI 1005 steel in different environments

As shown in Fig. 2, overall comparison of ln k_p values for the steel exposed to ethanol combustion and to dry air at different temperatures shows significantly considerable differences, suggesting little difference in oxidation resistance of the steel since there is considerable scatter in the values (Fig. 2). The scatter on the rate constants for mild steel oxidized in dry air is attributed to blistering of oxide scales. Similar discrepancies have been observed by Jha et al. [14] during oxidation studies in low alloy steels oxidized in high pressure oxidative environments from 700 to 1000 °C for oxidation times 10–250 hours whereas for steel oxidized in ethanol the scatters was attributed to the breakaway oxidation observed in the second parabolic regime at 800 °C after oxidizing for 4 hours. Furthermore, the activation energy for low carbon steel (Fe–0.04C–0.2Mn–0.02Si) was found to be 274 kJ/mol in 10%CO_2–90%N_2 at temperature range of 950–1150 °C [8]. Lee et al. [15] studied oxidation of low carbon steel (Fe–0.04C–0.015Mn–0.26Si) in 112% air–fuel (CH_4) combustion gas at the temperature of 700–1200 °C. The weight gain kinetics curves lead to parabolic curves at all temperatures and the activation energy is about 125 kJ/mol. It shows that the oxidizing gasses containing of water vapour and CO_2 significantly affect an activation energy.

In the present study, the activation energy of steel exposed to ethanol combustion was found to be 199 kJ/mol which is lower than that for steel exposed to dry air (224 kJ/mol). The lower activation energy shows the rapid increase in weight gain because H_2O–CO_2 gas mixtures resulted from ethanol combustion enhance iron ions diffusivity in the iron oxide by the discotioation process of H_2O and resulting hydrogen gas [11,12,16,17].

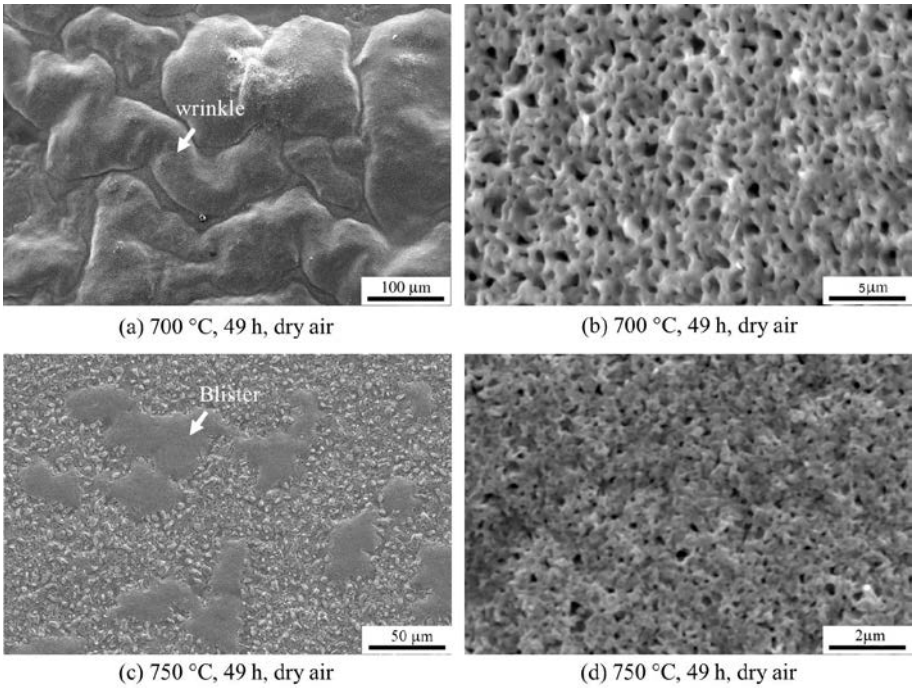

Fig. 3 SEM images morphologies of scales formed on mild steel; after 49 hours at 700 °C (a and b) and 750 °C (c and d) in dry air. A higher magnification (SEM images are show on the right side)

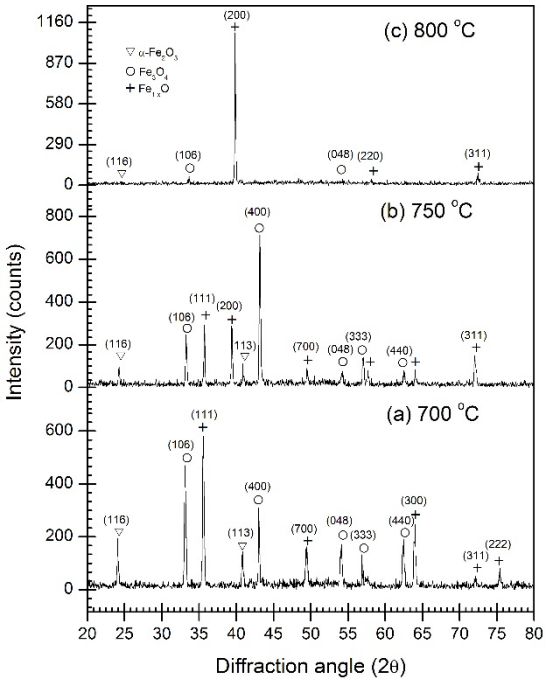

Fig. 4 XRD patterns taken from sample oxidized in dry air after 49 hours at (a) 700, (b) 750 and (c) 800 °C

3.2 Surface Morphologies Examinations

Fig. 3 shows surface morphology of steel oxidized in dry air at 700 and 750 °C for 49 hours. The XRD analyses of scale structures (Fig. 4), revealed wustite ($Fe_{1-x}O$), magnetite (Fe_3O_4) and hematite (α-F_2O_3) in the scale with the heights of the peaks representing wustite at 700 °C (Fig. 4a). As the temperature was increased to 750 and 800 °C, the heights of the peaks representing magnetite increased markedly (Fig. 4b and c). The surface of the steel is covered by wrinkled scale and shows hollow structures with a complete absence of whiskers (Fig. 3b and d). Wrinkle and blister scale were observed in dry air at 700 °C for 1–49 hours and at 750 °C for 1–25 hours (Fig. 3a and c). After short-term exposures, blisters start to form and the scale structure becomes irregular. Observing of the surface morphology at room temperature, blisters usually appear spotty, like pockmarks as shown in Fig. 3c. Chen and Yuen have described the formation of blisters and different layered scale structures very well [18].

Stresses due to different diffusion coefficients of iron and oxygen, different thermal expansion coefficients of the oxide scale and the steel and the plasticity of the oxide scale are factors causing wrinkles of the scale [19]. As shown in Fig 5a, the wrinkling of scale develops into buckling, leading to detachment of scale from the outer layer of hematite. A layer of coarser columnar grains with amount of porosity occupies a large part of the oxide thickness and at the oxide/gas interface is observed (Fig. 5b).

As the temperature was increased up to 800 °C for 49 hours, the blister scale disappeared and was replaced by rough-large grained structures. The rough-grained oxide can be distinguished as hematite (α–Fe_2O_3), as shown in (Fig. 6a).

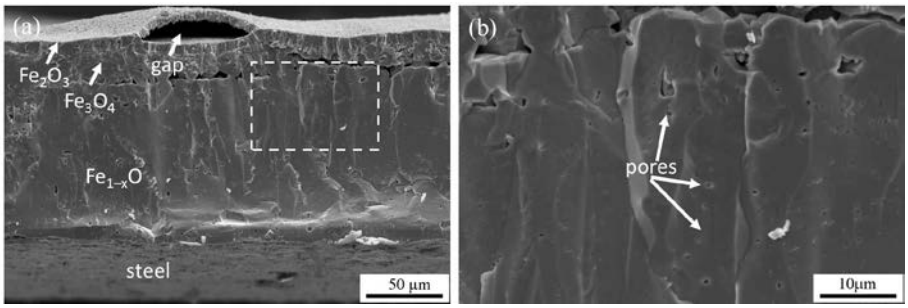

Fig. 5 SEM of Fracture surface of cross-sectional scale formed on steel at 750 °C for 25 hours in dry air: (a) overall figures and (b) higher magnification of square dash lines (a) showing columnar structure with many pores formed in the scale

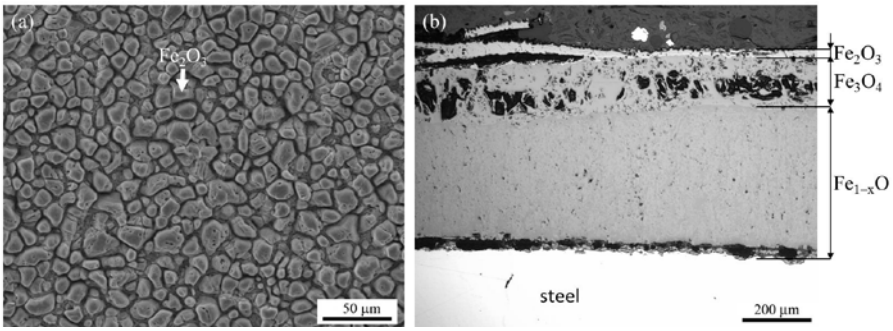

Fig. 6 (a) SEI image of surface morphology and (b) Optical micrograph of cross-sectional scale on the steel oxidized in dry air at 800 °C for 49 hours

In addition, the thickness of α–Fe_2O_3 is less uniform demonstrating that wrinkling is not caused by oxide intrusions or variations of the α–Fe_2O_3 growth rate from place to place (Fig. 6b).

3.3 Mechanism of Pyramidal Iron Oxide Scale Formation in Ethanol Combustion Products

Evolutions of iron oxide growth on the steel oxidized in ethanol combustion for 1 hour to 49 hours periods were examined by means of SEM (Fig. 7). At 700 °C after about 1 hour, the scale surface developed small-grained oxide growth with some fine oxide flakes growing on it (Fig. 7a). After an oxidation time of 9 hours, the initial flat surface developed into a rough surface comprised of large-grained oxide particles (Fig. 7b). Longer oxidation times (25 hours) resulted in another flat surface with facet-grained oxide shape (Fig. 7c). After oxidizing for 25 hours, some zones having large-grained oxide particles disappeared and reappeared as facet-grained oxide, as if the large-grained oxide particles have been incorporated in the dense faceted external magnetite layer. The cause for this is surface diffusion which remains active and flattens the surface with the thickening of magnetite and magnetite's progressive embedding into the oxide scale. This process has been described in detail by Peraldi et al. [20].

As the temperature oxidation was increased up to 750 °C for 1 hour, the large-grained oxide rapidly grew with some large flakes growing on it (Fig. 7d). Furthermore, for an oxidization time of 9 hours, the small undulating surface developed regularly into a rough surface comprised of small-pyramidal oxide growths (Fig. 7e). After longer exposure times (25–49 hours), the oxide grains initially showed pyramidal shapes, comprised of a mixture of smooth facets with small growing ledges and the oxide grains grew into larger pyramidal grains (Fig. 7f). When the temperature is increased to 800 °C, the mechanisms of pyramidal oxide growth are accelerated with the increase of exposure times, as shown in Fig. 7(g–i). It can be concluded that the growth of pyramidal oxide grain significantly depends on both the temperature and time in ethanol combustion.

With all oxide grains visible on the surface, it can clearly be observed that the pyramidal grains grew from the scale-steel interface with columnar grain structure (Fig. 8). In addition, the thin wustite develops with generation of many pores. Gesmundo and Hou [21] have stated that the formation of pores is generated by two processes, i.e., the oxide growth and any unbalanced flux of the metal components in the alloy. It is believed that wustite grains were formed at the beginning of the reaction, but magne-

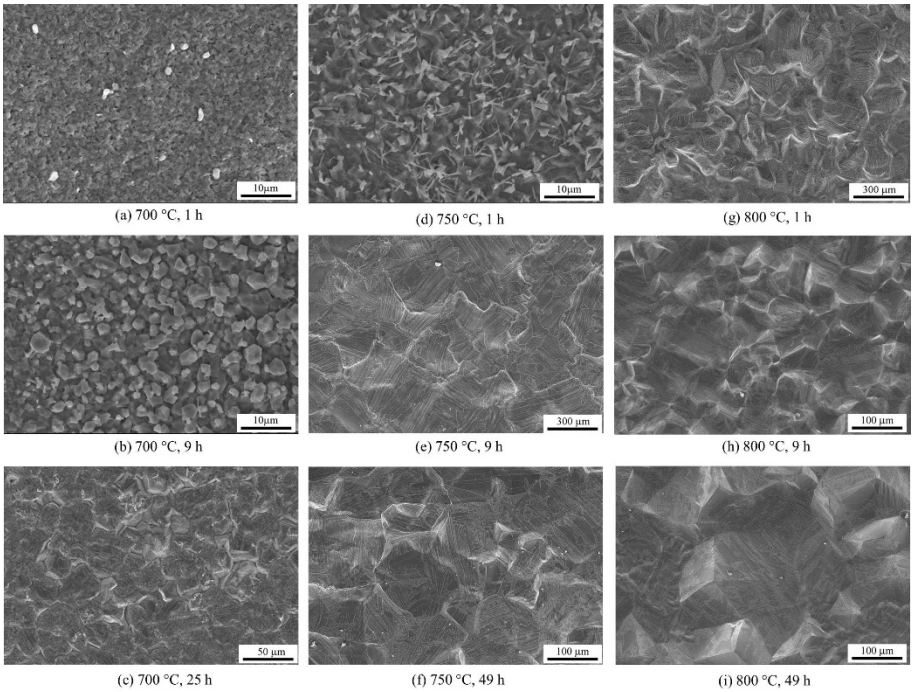

Fig. 7 SEI images of surface morphologies of scales formed on the steel exposed to ethanol combustion product at 700 °C, 750 °C and 800 °C

tite grains had grown faster than those of the wustite grains. For longer exposure times (at 700 C for 49 hours and at 750 and 800 °C for 25–49 hours), many pores can be observed in the inner layer near steel substrate. The thin layer containing many pores is the visible wustite layer, as shown in Fig. 9a.

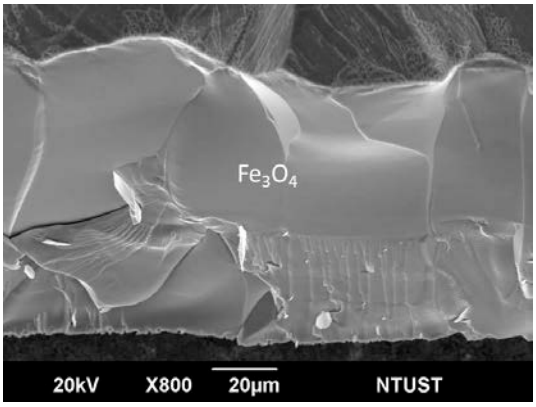

Fig. 8 SEM of fractured cross-section of scale formed on the steel exposed to ethanol combustion product at 800 °C after 4 hours showing the columnar structure of the magnetite

As shown in Fig. 1, when the steel was exposed to ethanol at 800 °C for 4 hours, the oxidation kinetics was found to be a rapid increase in mass-gain, leading to breakaway oxidation. The breakaway oxidation can possibly be attributed to carbon deposition in the scale [22,23]. This finding is evident with EDS elemental analyses mapping in the scale of the steel exposed to ethanol combustion product at 800 °C after 9 hours exposure. The elemental mapping reveals that carbon deposits in the crack path in the magnetite−wustite layer (Fig. 9b). Some previous studies show that the effect of CO_2 has a significant contribution in the formation of carbon deposition that was found in the iron oxide [22–25]. Pritchard et al. [23] studied mild steel oxidation in H_2O–CO_2 mixtures at 500 °C for 500 hours. They observed breakaway oxidation after an incubation period and the breakaway was initiated by a hydrogen effect such as accumulation of hydrogenous gas at the scale-metal interface.

Table 2 EDS's analysis results detecting carbon deposition in the scale on the specimen oxidized in ethanol combustion product at 800 °C for 49 hours

Location	Elemental composition (at.%)		
	Fe	O	C
1	74.94	23.88	1.17
2	77.35	21.64	1.01
3	63.36	23.95	12.70
4	63.11	30.22	6.67
5	58.21	31.76	10.03
6	77.56	21.47	0.97

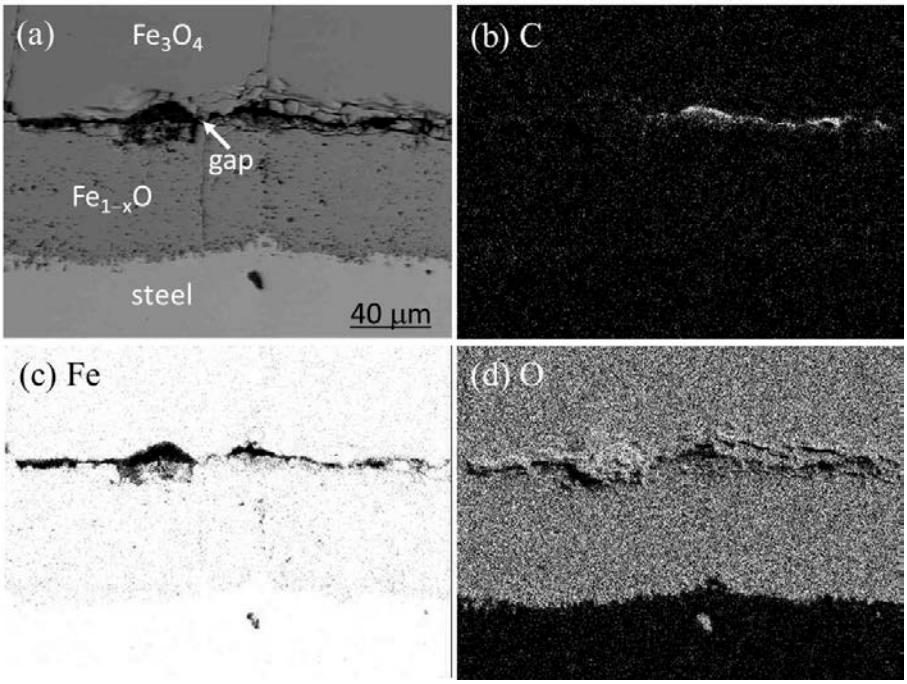

Fig. 9 BEI of oxide layer formed on the steel oxidized in ethanol combustion product at 800 °C for 9 hours and (b–d) corresponding to mapping of elemental concentration of C, Fe and O

The mechanisms of carbon deposition have been explained in detail by Gibbs [24]. The carbon formation is obviously coupled with the formation of magnetite. Oxide scales composed of wustite show no additional carbons in the oxide. SEM observation of cross-sectional scale on the steel after oxidizing for 49 hours (Fig. 10a and b) and EDS's analysis results detected a carbon contents (at.%) in the scale (Table. 2).

As shown in Fig. 9a, a large number of pores generated within the original oxide scale were attributed to coalescence of vacancies arising from Fe-atoms entering the region of the oxide-metal interface. CO and CO_2 molecules could not diffuse inside the wustite crystals because their solubilities are very weak in $Fe_{1-x}O$ [25]. Some cracks and pores observed gave facility in favoring the free access of carbon dioxide to the inner oxide, as well as the concurrent leaving of carbon monoxide. The presence of carbon close to the wustite–magnetite interface during protective oxidation lends support to the Gibbs theory [24] that the initially formed Fe_3O_4 layer develops microcracks or micropores. Both protective and breakaway scales are magnetite (Fe_3O_4), and are formed mainly by the reaction as follows [24]:

$$3Fe+4CO_2 \rightarrow Fe_3O_4+4CO \quad (1)$$

Some oxide may be formed from water vapour oxidation. Carbon deposited in the oxide is thought to arise from CO liberated by the reaction (1). This CO is, according to the Boudouard reaction (2):

$$2CO \rightarrow CO_2+C \quad (2)$$

The process of carbon deposition plays an important role in the nucleation and growth of breakaway oxidation. The observed carbon deposition leads to an increase of the weight gain and eventually leads to generating of stress within the inner oxide layer which could cause cracking of the outer scale and the initiation of breakaway oxidation stated to occur.

The growths of pyramidal grains of magnetite scale with a cubic morphology after longer exposure times are found in ethanol oxidation (Fig. 7f and i). The pyramidal structures are similar to those observed by Schmid et al. [26] in pure iron under pressure of H_2O 667 Pa at 700 °C and Chen and Yuen [18] in low carbon steel under 17%H_2O-N_2 at 900 °C. The explanation for pyramidal grain formation is initiated by nucleation of the large grained-oxide island on the surface and a high rate of arrival of iron cations on the surface provides the mechanism of islands formation. As the island grows, Fe atoms from the wustite layer diffused outward. Outward Fe diffusion could be one major means for long-range Fe supply. Furthermore, Fe atoms beneath the wustite/metal interface could diffuse to the growing interface due to shorter diffusion length. Because the pyramidal like grain structure comes from a columnar grain structure, thus its grain-growth process is initiated by secondary grain growth [27].

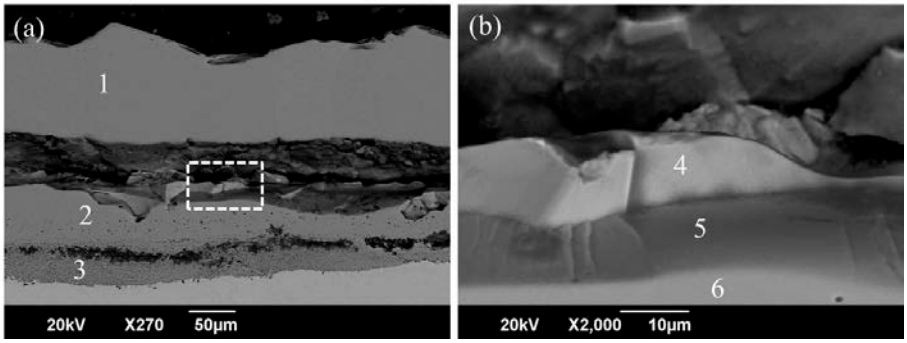

Fig. 10 BEI of cross-sectional micrograph of scale formed on the steel oxidized in ethanol at 800 °C for 49 hours and (b) higher magnification of panel (a) showing carbon deposition in the scale

A comparison of the molar volumes of wustite and magnetite, shows that magnetite has a molar volume about 10% smaller than wustite, i.e., at dry conditions $V_m(FeO)$ = 12.61 cm^3/mol_{oxygen}, and $V_m(Fe_3O_4)$ = 11.17 cm^3/mol_{oxygen} [26]. Assuming similar properties at higher temperatures, the rearrangement of iron atoms in the wustite structure will lead to tensile stresses within the oxide. Those stresses will arise in the confined wustite scale, assisting in the breakup of the oxide scale. In addition, iron produced from the breakdown of wustite into magnetite will diffuse along the new grain boundaries to the surface, where it oxidizes to form magnetite. With thickening of the scale, although lattice diffusion is still fast, surface diffusion is becoming more dominant. Furthermore, after longer exposure times the oxide scale changes its growth mode and establishes a pyramidal growth structure. After further transformation of the wustite, the morphology of the oxide scale can be explained by continuous formation of magnetite crystals from the wustite phase. Although no breakdown reaction of wustite into magnetite and iron was found. However, magnetite formation was initially preceded by a breakdown reaction of wustite.

4. CONCLUSION

The oxidation kinetics of steel oxidized in ethanol combustion product is higher than that those of steel oxidized in dry air at temperatures ranging from 700–800 °C for 49 hours. The presence of H_2O and CO_2 gasses resulted by ethanol combustion in tube chamber affected the growth of morphologies oxide scale. The surfaces of the scales growing on the steel oxidized in ethanol combustion exhibited pyramidal grain structures with an increase of time and temperature oxidation. Columnar grain structures are observed in the wustite layer (in dry air) and magnetite (in ethanol combustion). The effect of CO_2 from ethanol combustion product was very influential on the oxidation of steel at the higher temperature oxidation (i.e. 800 °C). The carbon deposition found in the magnetite-wustite layer for an oxidation time of 9 hours is believed to favor the breakaway oxidation.

5. ACKNOWLEDGMENTS

The authors are very grateful to the Kemerinstekdikti of Republic of Indonesia for financially supporting the present work via the basic research grant scheme under contract no. 065/SP2H/LT/DRPM/2019.

6. REFERENCES

[1] Szklo A., Schaeffer R. and Delgado F., Can one say ethanol is a real threat to gasoline? Energy Policy, Vol. 35, 2007, pp. 411–5421.

[2] Ashraf E., Investigations on the effects of ethanol–methanol–gasoline blends in a spark-ignition engine: Performance and emissions analysis, Eng. Sci. Technol, Int. J., Vol. 18, 2015, pp. 713−719.

[3] Yang, H. H., Liu, T. C., Chang, C. F. and Lee, E., Effects of ethanol-blended gasoline on emissions of regulated air pollutants and carbonyls from motorcycles, Appl. Energy, Vol. 98, 2012, pp. 281−286.

[4] Yuksel F. and Yuksel B., The use of ethanol–gasoline blend as a fuel in an SI engine. Renew. Energy, Vol. 29, 2014, pp. 1181−1191.

[5] Agarwal A. K., Karare H. and Dhar A., Combustion, performance, emissions and particulate characterization of a methanol–gasoline blend (gasohol) fuelled medium duty spark ignition transportation engine. Fuel Proc. Technol., Vol. 121, 2014, pp. 16−24.

[6] Yoo Y. H., Park I. J., Kim J. G., Kwak D. H. and Ji W. S., Corrosion characteristics of aluminum alloy in bio-ethanol blended gasoline fuel: Part 1. The corrosion properties of aluminum alloy in high temperature fuels. Fuel, Vol. 90, 2011, pp. 1208–1214.

[7] Wang C. J. and Badaruddin M., The dependence of high temperature resistance of

aluminized steel exposed to water-vapour oxidation, Surf. Coat. Technol., 205, 2010, pp. 1200–1205.

[8] Chen R. Y. and Yuen W. Y. D., Oxidation of low-carbon steel in $17H_2O$-N_2 at 900 °C. Metallur. Mater. Trans. A, Vol. 40, 2009, pp. 3091–3107.

[9] Abuluwefa H. T., Guthrie R. I. L. and Ajersch F., Oxidation of low carbon steel in multicomponent gases: Part I. Reaction mechanisms during isothermal oxidation. Metallur. Mater. Trans. A, Vol. 28, 1997, pp. 1633–1641.

[10] Dudziak T., Jura K., Polkowska A., Deodeshmukh V., Warmuzek M., Witkowska M., Ratuszek W. and Chrusciel K., Steam Oxidation Resistance of Advanced Steels and Ni-Based Alloys at 700 °C for 1000 h. Oxid. Met., Vol. 89, 2018, pp. 755–779.

[11] Yuan J., Wang W., Zhu S. and Wang F., Comparison between the oxidation of iron in oxygen and in steam at 650–750°C. Corros. Sci. Vol. 75, 2013, pp. 309–317.

[12] Wang J., Meng L., Fan Z., Liu Q. and Tong Z., Mechanism and modelling of CO2 corrosion on downhole tools, R. Soc. Open Sci. 6, 2019, 181899.

[13] ASTM G54-84, Standard Practice for Simple Static Oxidation Testing, ASTM International, West Conshohocken, PA, 1996.

[14] Jha R., Haworth C. W. and Argent B. B., The formation of diffusion coatings on some low-alloy steels and their high temperature oxidation behaviour: Part 2. Oxidation studies. Calphad, Vol. 25, 2001, pp. 667–689.

[15] Lee V. H. J., Gleeson B. and Young D. J., Scaling of carbon steel in simulated reheat furnace atmospheres. Oxid. Met., Vol. 63, 2005, pp. 15–31.

[16] Quadakkers W. J. and Żurek J., Oxidation in Steam and Steam/Hydrogen Environments. Shreir's Corros. 2010, pp. 407–456.

[17] Gheno T., Monceau D., Young D. K., Mechanism of breakaway oxidation of Fe–Cr and Fe–Cr–Ni alloys in dry and wet carbon dioxide. Corros. Sci. Vol. 64, 2012, pp. 222–233.

[18] Chen R.Y. and Yuen W.Y.D., Review of the high-temperature oxidation of iron and carbon steels in air or oxygen. Oxid. Met., Vol. 59, 2003, pp. 433–468.

[19] Stott F.H., Wood G.C. and Stringer J., The influence of alloying elements on the development and maintenance of protective scales. Oxid. Met., Vol. 44, 1995, pp. 113–145.

[20] Peraldi R., Monceau D. and Pieraggi B., Correlations between growth kinetics and microstructure for scales formed by high-temperature oxidation of pure nickel. I. morphologies and microstructures. Oxid. Met., Vol. 58, 2002, pp. 249–273.

[21] Gesmundo F. and Hou P. Y., Analysis of pore formation at oxide–alloy interfaces—II: Theoretical treatment of vacancy condensation for immobile interfaces. Oxid. Met., Vol. 59, 2003, pp. 63–81.

[22] Shi J., Wang D. R., He Y. D., Qi H. B. and Wei G., Reduction of oxide scale on hot-rolled strip steels by carbon monoxide. Mater. Lett., Vol. 62, 2008, pp. 3500–3502.

[23] Pritchard A. M., Antill J. E., Cottell K. R. J., Peakall K. A. and Truswell A. E., The mechanisms of breakaway oxidation of three mild steels in high-pressure CO_2 at 500 °C. Oxid. Met., Vol. 9, 1975, pp. 181–213.

[24] Gibss G. B., A model for mild steel oxidation in CO_2. Oxid. Met., Vol. 7, 1973, pp. 173–183.

[25] Valette S., Denoirjean A., Tátard D. and Lefort P., C40E steel oxidation under CO_2: Kinetics and reactional mechanism. J. Alloys. Compd., Vol. 413, 2006, pp. 222–231.

[26] Schmid B., Aas N., Grong O. and Odegård R., High-Temperature Oxidation of Iron and the Decay of Wüstite Studied with in situ ESEM. Oxid. Met., Vol. 57, pp. 115–130.

[27] Thompson C. V., Grain growth in thin films. Ann. Rev. Mater. Sci., Vol. 20, 1990, pp. 245–268.